

Development of Negative Ion Based Neutral Beam Injector toward JT-60SA

Yutaka TANAKA, Masaya HANADA,
Kaoru KOBAYASHI, Masaki KAMADA and Masashi KISAKI¹⁾

Japan Atomic Energy Agency, Naka, 311-0193, Japan

¹⁾*Graduate School of Engineering, Tohoku University, Sendai, 980-8579, Japan*

(Received: 1 September 2008 / Accepted: 18 December 2008)

This paper reports recent R&D results on negative ion-based NBI for JT-60SA where 10 MW neutral beam is designed to inject for 100 seconds. There are major two issues such as improvement of voltage holding capability and reduction of the grid power loading of the JT-60U negative ion source with three acceleration stages. To improve the voltage holding capability, the breakdown location with the beam acceleration was examined. In the upper ion source, breakdowns in the first gap were dominated by the cesium contamination. In the lower ion source, breakdowns occurred in the second and third gaps, since the beam optics was not optimized. Optimization of the beam perveance and reduction of the cesium contamination are required toward JT-60SA. To reduce the grid power, outward deflection of outmost beamlets, due to space charge of the inner beamlets, was suppressed by optimizing the acceleration electric field. This allowed to reduce the power loading of GRG. After the reduction of the power loading, injection pulse length was extended up to 30 s. The water temperature rise of the components saturated at 25 s. This shows that existing water-cooled components can be reused for JT-60SA.

Keywords: JT-60SA, negative ion source, voltage holding capability, breakdown, beamlet, field shaping plate

1. Introduction

Negative ion based NBI (N-NBI) has been used in JT-60U to heat the plasma and to drive the non-inductive plasma current [1]. In ITER, N-NBI becomes a main heating system, and its development is in progress [2]. In JT-60SA project, which started to support ITER and to demonstrate steady state high beta plasma for DEMO, N-NBI is required to inject 10 MW D^0 beams at beam energy of 500 keV and pulse duration of 100 s [3].

With two negative ion sources on JT-60U, the achieved highest injection power and longest injection time were 5.8 MW at 400 keV for 0.9 s and 30 s at 1 MW, 300 keV, respectively [1]. To meet the requirements of JT-60SA, the JT-60U negative ion sources should be upgraded. The injection power and time are restricted by voltage holding capability and the power loading of the multi-aperture acceleration grid. Therefore, a poor voltage holding capability and high grid power loading should be overcome toward JT-60SA.

The achieved voltage holding capability of the JT-60U negative ion source is 450 kV without the beam acceleration. With the beam acceleration, the voltage holding capability is degraded to 400 kV. In the previous study [4], it is confirmed that there is no particular weak acceleration stage occurring the breakdown. However, breakdown location with the beam acceleration has not been clarified yet. As the first step for improving the

voltage holding capability, the breakdown location in the multi-stage negative ion accelerator was examined on site of JT-60U by new diagnostics.

As for the grid power loading, the highest grid power was as high as 9 % of the accelerated beam power. For the long pulse injection, the grid power loading should be reduced to the acceptable level of 5 %. To reduce the grid power, the field shaping plate for suppressing the direct interception of high-energy D^- ions was newly designed and tested in the negative ion source. After the reduction of the grid power, injection pulse length was extended up to 30 s to study the feasibility of the long pulse injection.

2. Voltage holding capability with the beam acceleration

In the previous study, there is no particular weak acceleration stage occurring the breakdown in the case without the beam acceleration. However, the breakdown location has not been clarified yet in the case with the beam acceleration, where voltage holding capability is 80 % of that without the beam acceleration. Then, the breakdown location was identified in two negative ion sources (U and L ion sources) on JT-60U. Each of the ion sources is composed of semi-cylindrical shaped arc chamber with 122 cm in length and 68 cm in diameter and an electrostatic accelerator with three stages as

author's e-mail: tanaka.yutaka@jaea.go.jp

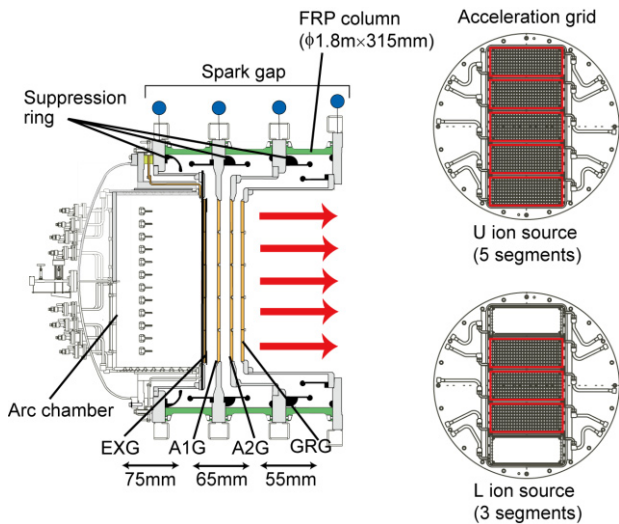


Fig. 1 Schematic view of the negative ion source. U and L ion sources have 5 and 3 segments of acceleration grids.

shown in Fig. 1. Cesium vapor is introduced from the cesium oven. The operation cesium rate to the arc chamber is $\sim 14 \mu\text{g/s}$. The accelerator is composed of grids with multi-apertures and large fiberglass reinforced plastic (FRP) insulators with 1.8 m in inner diameter. The accelerator has an extraction grid (EXG) and 3 acceleration grids (A1G, A2G, GRG). The same acceleration voltage is applied to each acceleration grids.

U and L ion sources are connected with a common acceleration power supply in parallel. To identify where the breakdowns were initiated, the time difference of lights emitted from the spark gaps, which were connected with each of the acceleration stages, was measured. As shown in Fig. 2, when a vacuum breakdown is initiated in the third acceleration gap, the total acceleration voltage is instantaneously applied to the other two acceleration gaps. If the applied voltage exceeds the rated voltage (170 kV) determined by length between the spark gaps, the discharge occurs at the spark gaps and emits the light. Figure 3 shows a typical time evolution of the lights when a breakdown occurs. Lights emitted from the spark gaps are labeled as U1, U2, U3, L1, L2, L3, where U and L indicate two ion sources, and 1, 2, 3 indicate acceleration stages. Lights at U1, U2, L1, L2 increase very quickly in an order of nano-second. This indicates that a vacuum breakdown occurs at U3 or L3. Since initiation of the lights of L1, L2 is earlier than that of U1, U2, initial location of the vacuum breakdown is identified to be L3.

Figure 4 shows time history of (a) breakdown voltage, (b) accelerated beam currents, (c) total introduced cesium amount and (d) fractions of breakdown locations in ‘2008 campaign. Voltage holding capability with the beam acceleration gradually increases from 320 kV to 370 kV. In this period, the voltage holding capability without the beam acceleration increased from 400 kV to 460 kV.

In the U ion source, the beam current (I_{acc}) was

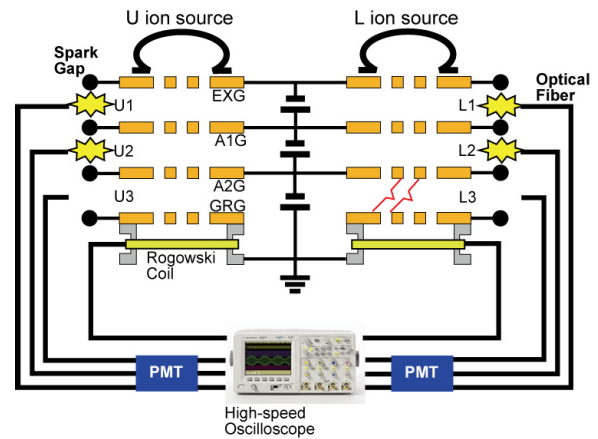


Fig. 2 Diagnostic system to identify the initial location of the vacuum breakdown.

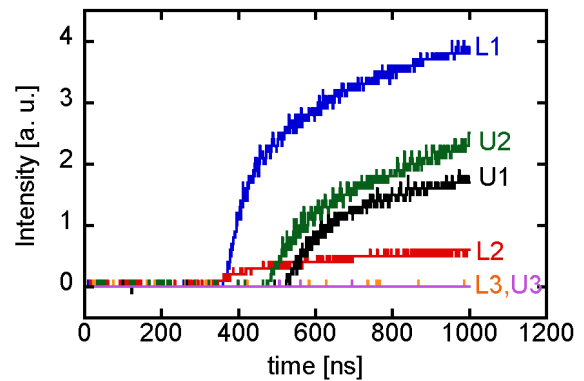


Fig. 3 Typical time evolution of light intensities emitted from the spark gaps.

increased with the enhancement of the acceleration voltage (V_{acc}) according to the child-Langmuir law, i.e., $I_{\text{acc}} \propto V_{\text{acc}}^{1.5}$ (see ‘U’ in Fig. 4 (b)). The cesium was introduced at the rate of $\sim 0.4 \text{ g/day}$. As shown in Figure 4 (d), the breakdowns occurred mainly in the second gap during 2/19-3/11, and then occurred in all acceleration gaps. The breakdown in the first gap relatively increased with the operation time. During 6/23-7/8, the fraction of the first gap tended to increase. This is due to the cesium contamination in the EXG served as cathode in the first gap, although more detailed study is required. The fraction of the breakdowns was the same as that without the beam acceleration although the fraction of the first gap relatively increased.

In the lower ion source, the filaments were broken after the first three weeks. For this reason, the input arc power was limited, so that the accelerated beam current was much lower than the optimum beam current for the acceleration voltage. In this case, the breakdown occurred mainly in the second and third gaps, and was largely different from that in the upper ion source where the beam optics was optimized. When the beam current is insufficient for the acceleration voltage, the ion beam is over-focused. Due to the over-focusing of the ion beam, the ion beams are intercepted by the intermediate grids, by

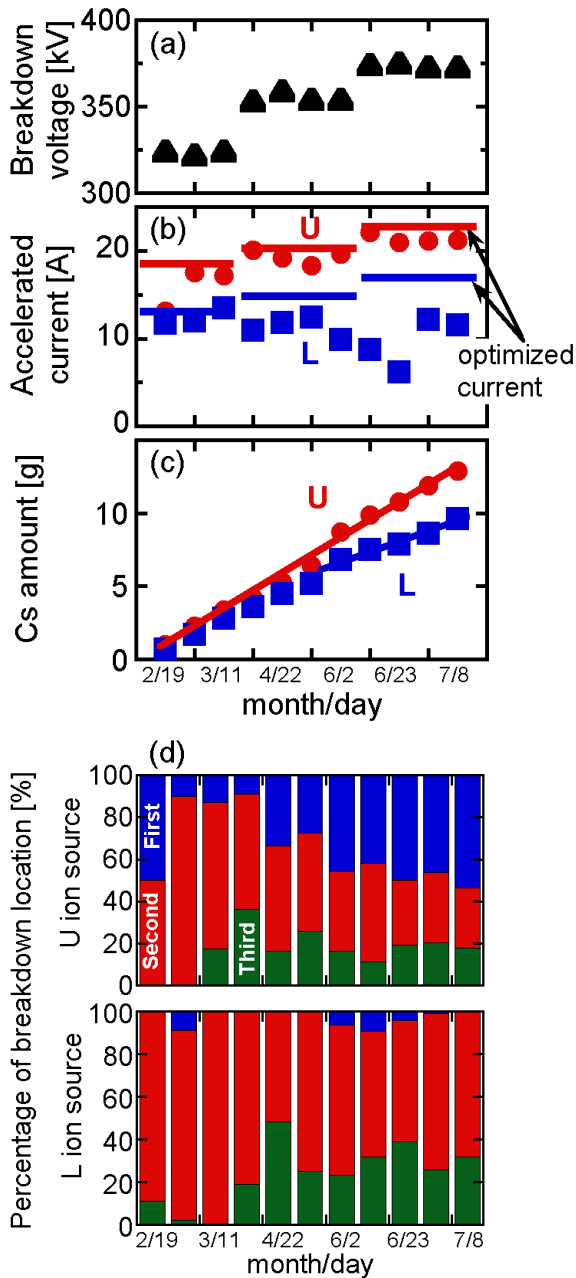


Fig. 4 Time history of (a) breakdown voltage, (b) accelerated beam current, (c) introduced cesium amount and (d) fractions of breakdown locations on U and L ion sources.

which the secondary electrons are generated. The impingement of the D^- ions and/or the secondary electrons might degrade the voltage holding capability.

Number of the breakdowns in the L ion source was larger by 20 % than that in the U ion source. This indicates that the breakdown is largely affected by the beam optics. However, the beam will be produced under the optimum perveance in JT-60SA, and the cesium flow into the accelerator is required to be suppressed to improve the voltage holding capability.

3. Reduction of Grid Power Loading

Thermal analysis shows that acceptable grid power

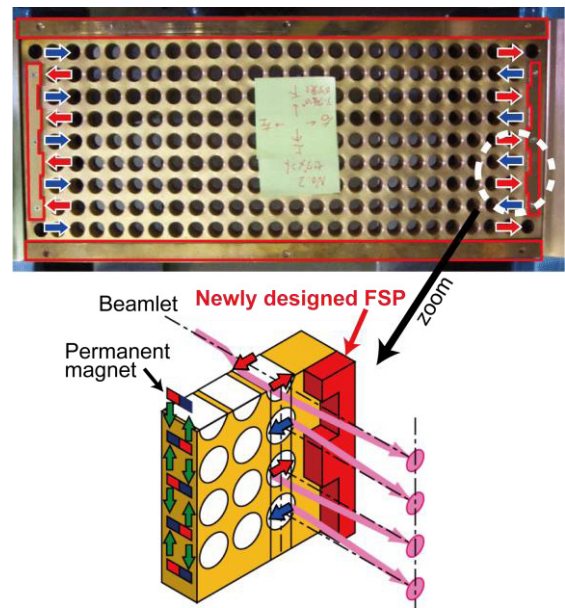


Fig. 5 A photograph of a sub-segment of EXG, and a schematic view of newly designed FSP. The deflection of beamlets caused by magnetic field is indicated by red and blue arrows.

loading for the 100 s injection is 1 MW that corresponds to 5 % of the acceleration beam power [5]. In last campaign, the highest power loadings obtained in U and L ion sources were 9 % and 7 % on GRG, respectively. So, the GRG power loading should be reduced $< 5\%$. In the previous study, it was found that the GRG power loading was mainly caused by the direct interception of outmost beamlets of D^- ions that were deflected outward due to the space charge of inner beamlets [6]. To suppress the direct interception of outmost beamlets, the focusing electric field for the outmost beamlets is formed by placing a field shaping plate (FSP) on EXG. Figure 5 shows a photograph of a sub-segment of the EXG and the schematic view of the developed FSP. The surface shape of the FSP on the side of aperture is corrugated to tune the distance between the grid aperture and the plate since the horizontal steering of the beamlets due to the dipole magnetic field in the EXG is reversed every row of the apertures. Since the thickness is fixed to be 1.5 mm due to the geometry limitation, the distance between the grid aperture and the FSP is designed using the simulation of beam trajectory at beam energy of 350 keV. Figure 6 shows the deflection angle of outmost beamlets as a function of the distance between an aperture and FSP. The allowed deflection angle, which is determined from the limitation of direct interceptions with GRG and the beam scraper located downstream, is from -4 mrad to -7 mrad. To satisfy this limitation, the distance between the aperture and the FSP for outward and inward beamlets are set to be 11 mm and 14 mm, respectively. The FSP on top and bottom in each of sub-segment is also designed to focus the outmost beamlets vertically using the simulation. The distance between the FSP and aperture

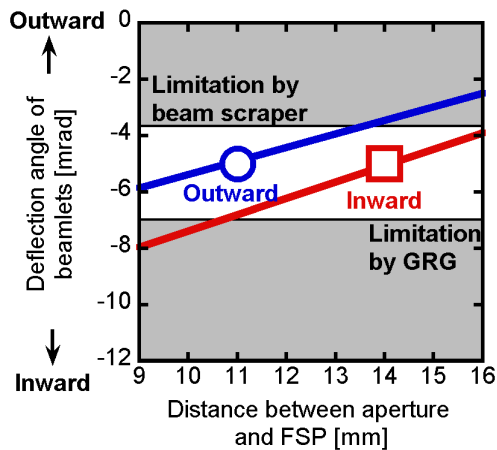


Fig. 6 Deflection angle of inward and outward beamlets. Each line indicates the simulation result. The distances shown by two symbols are selected in FSP.

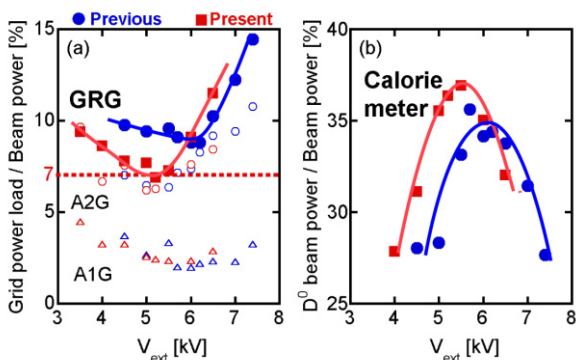


Fig. 7 (a) Grid power loading and (b) D^0 beam power normalized by the accelerated beam power. This data is obtained using the U ion source.

and the thickness of FSP are designed to be 13 mm and 1.0 mm, respectively.

Figure 7 (a) shows the experimental results of grid power of GRG on the U ion source as a function of the extraction voltage (V_{ext}). In this graph, the previous power loadings of GRG are shown for comparison. The power loadings of GRG with five grid segments are minimized by tuning the V_{ext} . By the FSP, the minimum power loading was reduced from 9 % to 7 % of the accelerated beam power. The reduction of the grid power loading allowed to increase the neutral beam power measured with calorimeter at the downstream of 17 m from the ion source. Figure 7 (b) shows neutral beam powers after neutralization. Two lines are obtained before and after the FSP installation. The neutral beam powers were maximized at a slightly higher optimum extraction voltage that minimized the power loading of GRG.

Similar dependence on the extraction voltage was obtained in the L ion source with central three grid segments, where the beam uniformity along the longitudinal direction was better than that in the U ion source with five grid segments. In the L ion source, the power loading of GRG was reduced from the previous

value of 7 % to acceptable level of 5 % by the FSP. This shows that the FSP can be used to reduce the grid power loading. In JT-60SA, the magnetic field configuration of the arc chamber will be changed to “tent-shaped filter configuration” where the beam uniformity has been successfully improved in the 10 A ion source [7]. By using FSP with the tent-shaped filter configuration in JT-60SA, the grid power loading could be reduced to the acceptable level.

After the reduction of the grid power loading, the injection pulse length was extended from 20 s to 30 s to study the feasibility of the long pulse injection. At neutral beam power of 2 MW, water temperature rise of the components such as ion source and residual ion dump was 40 °C and saturated at 25 s. This shows that existing water-cooled components can be reused for JT-60SA.

4. Summary

N-NBI developments such as improvement of voltage holding capability and reduction of the grid power loading were carried out toward JT-60SA.

In the U ion source, due to the cesium contamination in the EXG, the breakdowns in the first gap gradually increased with the operation time. In the L ion source, the breakdown occurred mainly in the second and third gaps, since the beam optics was not optimized. Optimization of the beam perveance and reduction of the cesium contamination are required to improve the voltage holding capability.

FSP was placed on EXG to tune the outward deflection of outmost beamlets. The power loading of GRG was reduced from 9 % to 7 %, and from 7 % to 5 % of the accelerated beam power on the U and L ion sources. In JT-60SA, by using FSP with the tent-shaped filter configuration, where the beam uniformity has been improved, the grid power loading could be reduced to the acceptable level of 5 %.

The injection pulse length was extended up to 30 s. The water temperature rise of the components was saturated at 25 s. This shows that existing water-cooled components can be reused for JT-60SA.

Acknowledgment

The authors would like to thank other members of JT-60U NBI Heating Group for their valuable discussion. They are also grateful to Dr. T. Tsunematsu and Dr. N. Hosogane for their support and encouragement.

- [1] Y. Ikeda, *et al.*, Nucl. Fusion, **46**, S211, (2006).
- [2] R. S. Hemsworth *et al.*, Rev. Sci. Instrum, **79**, 02C109 (2008).
- [3] Y. Ikeda, *et al.*, Fusion Eng. Des., **82**, 791 (2007).
- [4] K. Kaoru, Proc. 23rd International Symposium on Discharges and Electrical Insulation in Vacuum, Bucharest, Romania, 2008, p. 541.
- [5] M. Hanada *et al.*, Rev. Sci. Instrum., **79**, 02A519 (2008).
- [6] M. Kamada *et al.*, Rev. Sci. Instrum., **79**, 02C114 (2008).
- [7] M. Hanada *et al.*, Nucl. Fusion, **47**, 1142, (2007).